High Sensitivity Strain and Temperature Sensing With Cascaded Sagnac Interferometer Based on Harmonic Vernier Effect

Xin DING[1,2,3], Shen LIU[1,3], Mengjie WANG[4], Nan CHEN[5], Weiguan ZHANG[2,3], and Yiping WANG[1,3*]

[1]*Key Laboratory of Optoelectronic Devices and Systems of Ministry of Education/Guangdong Province, College of Physics and Optoelectronic Engineering, Shenzhen University, Shenzhen 518060, China*

[2]*Guangdong Laboratory of Artificial Intelligence and Digital Economy (Shenzhen), Shenzhen 518107, China*

[3]*Guangdong and Hong Kong Joint Research Centre for Optical Fiber Sensors, Shenzhen University, Shenzhen 518060, China*

[4]*School of Optical-Electrical and Computer Engineering, University of Shanghai for Science and Technology, Shanghai 200093, China*

[5]*School of Electrical Engineering, Nantong University, Nantong 226019, China*

[*]Corresponding author: Yiping WANG E-mail: ypwang@szu.edu.cn

Abstract: To further improve sensor sensitivity, a strain and temperature sensor based on the harmonic Vernier effect with cascaded Sagnac interferometers (SIs) is proposed. Through a combination of simulation and experimentation, it is shown that the basic Vernier effect can be realized when the lengths of the polarization-maintaining fiber (PMF) in two SIs are slightly different. Furthermore, the first-order harmonic Vernier effect can be achieved when the lengths of two PMFs are approximately integer multiples. This sensor, leveraging the harmonic Vernier effect, demonstrates higher sensitivity. Compared to a single SI, the strain sensitivity based on the basic Vernier effect is improved to 61.93 pm/με with a magnification factor of 7.6, and the temperature sensitivity is improved to 14.29 nm/℃ with a magnification factor of 9.4. For the first-order harmonic Vernier effect, the strain sensitivity increases to 146.35 pm/με with a magnification factor of 18, and the temperature sensitivity increases to 24.92 nm/℃ with a magnification factor of 16.5. Additionally, the sensor based on the harmonic Vernier effect exhibits good stability in strain and temperature measurement. Unlike the basic Vernier effect, the harmonic Vernier effect does not require strict control of the reference and sensing interferometer lengths, further increasing sensitivity. Due to its simple structure and low cost, the proposed sensor shows significant potential for applications in high-precision measurement engineering and medical treatment.

Keywords: Cascade Sagnac interferometers; harmonic Vernier effect; strain and temperature measurement; polarization-maintaining fiber

Citation: Xin DING, Shen LIU, Mengjie WANG, Nan CHEN, Weiguan ZHANG, and Yiping WANG, "High Sensitivity Strain and Temperature Sensing With Cascaded Sagnac Interferometer Based on Harmonic Vernier Effect," *Photonic Sensors*, 2025, 15(3), 250319.

Received: 2 August 2024 / Revised: 18 October 2024

DOI: 10.1007/s13320-025-0762-4
Article type: Regular

1. Introduction

With the continuous progress of the optical fiber sensing technology, optical fiber Sagnac interferometers (SIs) are increasingly used in various fields, such as fiber filters [1–3], couplers [4, 5], hydrophones [6], and gyroscopes [7–10]. The sensitivity of the SI can be improved by embedding a special fiber in the Sagnac loop, changing the structure of the Sagnac ring, or coating other materials. Dong *et al*. [11] proposed a strain sensor based on the SI, which was composed of the polarization-maintaining photonic crystal fiber (PM-PCF). The sensor exhibited the strain sensitivity of 0.23 pm/με. In order to realize two-parameter measurement, Kim *et al*. [12] reported the strain and temperature sensor of the elliptical hollow photonic band gap fiber based on an SI. The sensor exhibited the sensitivity of −0.81 pm/με over a strain range of 0 με–1 000 με and the temperature sensitivity of 3.97 pm/℃ over a temperature range of 20 ℃–90 ℃. However, sensors based on a single SI are limited by fiber inherent properties in terms of sensitivity and responsiveness [13]. To address the problem of low sensitivity in the traditional sensors, recent advancements have leveraged the remarkable properties of the optical Vernier effect. The optical Vernier effect enhances the sensitivity of the sensor by incorporating an interferometer with a similar interferometric frequency, typically arranged in a cascaded configuration. This effect has led to improvements in sensors by several orders of magnitude. Numerous studies have demonstrated the high sensitivity characteristics achieved through the Vernier effect, showcasing significant technological progress and innovative developments in this field. Chen *et al*. [14] reported a highly sensitive temperature and pressure sensor based on the cascade Fabry-Pérot interferometer (FPI) and SI. The sensor achieved a sensitivity of 23.14 nm/℃ and 49.2 nm/MPa for temperature and pressure measurement, respectively, with a sensitivity magnification of 13.4 times and 12.2 times, respectively. Ding *et al*. [15] proposed a high sensitivity temperature sensor based on the Vernier effect and using the cascaded high birefringent fiber (HBF) as the sensitive unit. In order to construct the sensor, a longer HBF and a shorter HBF were selected to form two SIs as the sensing arm and the reference arm. In the temperature range of 20 ℃ to 24 ℃, the sensor exhibited the temperature sensitivity of −43 nm/℃ and successfully achieved a sensitivity amplification effect of 24.96 times. Jia *et al*. [16] reported a high-sensitivity temperature sensor based on the Vernier effect, which cascaded the SI and Mach-Zinder interferometer (MZI). The SI composed of a polarization-maintaining fiber (PMF) was used as the temperature sensing arm, and the dual-channel MZI was used as the reference arm. The sensor has high temperature sensitivity of 14.3 nm/℃ and a magnification of 8.51 over a temperature range of 20 ℃–22 ℃. In addition to cascading the sensing arm and the reference arm, there have been some fiber-optic Vernier sensors based on parallel structures. For example, Lin *et al*. [17] proposed a fiber-optic gas pressure sensor to realize high sensitivity measurement by using the Vernier effect. The sensor consisted of two integrated parallel MZIs that were manufactured by fusing a small section of the bilateral empty fiber between two short multimode fibers. The sensor demonstrated the sensitivity of −60 nm/MPa over a gas pressure test range of 0 MPa–0.8 MPa. Nan *et al.* [18] proposed a novel parallel structure fiber FPI, specially designed for ultra-sensitive strain measurement. The sensor consisted of an open chamber and a closed chamber, where the open chamber FPI was used for the sensing function and the closed chamber FPI was used as a reference, resulting in the ultra-high strain sensitivity of −43.2 pm/με. In addition, Zhang *et al*. [19] proposed a shin-fiber Michelson interferometer high sensitivity bending sensor based on the Vernier effect. The sensor was made of a dual-core fiber and a small segment of a dual-hole fiber through

precision splicing, achieving the bend sensitivity of 38.53 nm/m^{-1}.

Sensors in [16–19] were based on the basic optical Vernier effect, which meant that there was a small optical path difference between the two interferometers, and the outer envelope of the spectrum was utilized to enhance sensitivity. In fact, there was also the harmonic Vernier effect, first proposed by Gomes *et al*. [20] in 2019. The optical path length of one interferometer was increased by a multiple (i times) of the optical path length of the second interferometer, thereby using a larger optical path difference to achieve greater enhancement in sensitivity. Subsequently, Gomes *et al*. [21] used hollow microspheres and a section of the fiber as two FPIs to generate the harmonic Vernier effect, proving the optical path conditions for realizing the harmonic Vernier effect. This effect produced a higher magnification, proportional to the order of harmonics. Yang *et al*. [22] proposed a simple gas pressure sensor, which was composed of two hollow silica capillary tubes fused together. The harmonics of the optical Vernier effect were observed by properly adjusting the length of the silica capillary tube, with gas pressure sensitivity of 80.8 pm/kPa in the range of 1 kPa–101 kPa. Luo *et al*. [23] proposed a high-sensitivity parallel gas pressure sensor based on the harmonic Vernier effect. The sensor was composed of two 75 μm hollow capillary tubes, which served as the sensing chamber and the reference chamber, respectively, and achieved the pressure sensitivity of 279.52 pm/kPa with a magnification of 67.7. He *et al*. [24] proposed a high-sensitivity temperature sensor based on the harmonic Vernier effect. This sensor primarily consisted of two segments of the PMF and obtained the sensitivity of 40.73 nm/℃ within the temperature range of 28 ℃–44 ℃. While the harmonic Vernier effect resulted in higher sensitivity, it also presented challenges, such as the complex structure preparation, low mechanical strength, and poor repeatability. To address these issues and further enhance sensor sensitivity while overcoming the basic Vernier effect's optical path difference matching challenges, this paper proposes a simpler cascaded SI fiber sensor based on the harmonic Vernier effect. In this paper, a harmonic Vernier effect can be achieved when the PMF length of one Sagnac loop is an integer multiple of the PMF length in another Sagnac loop with a small deviation. Relying on the harmonic Vernier effect, the sensor can achieve a higher sensitivity amplification effect and achieve the goal of high sensitivity measurement.

2. Theory and simulations

2.1 Schematic and theory

2.2.1 Fiber SI principle

A single SI structure composed of the PMF is shown in Fig. 1, whose transmission strength is determined by the phase difference between two reverse-transmitted waves [25]. By means of a 2×2 3 dB coupler, the light emitted by a light source is split into two beams, which are then introduced into the Sagnac loop made of the PMF and transmitted in the opposite direction within the loop. Due to the difference in the refractive index (RI) between the fast axis and slow axis in the PMF, the two beams of light passing through the fiber form a phase difference during propagation. Interference occurs when the two light waves re-enter the fiber coupler, which is captured and recorded by the spectrometer. The intensity of the light field is a cosine function of the reciprocal wavelength, and the equation is as follows:

$$I = \frac{1}{2} - \frac{1}{2}\cos\theta \tag{1}$$

where θ represents the phase difference, which can be adjusted by the polarization controller, calculated by the following equation:

$$\theta = \frac{2\pi BL}{\lambda} \tag{2}$$

where L represents the PMF length, λ represents the wavelength of incident light, and B represents the effective RI difference between the fast axis and slow axis in the PMF, also known as the

birefringence coefficient of the PMF. When the phase difference meets the following conditions:

$$\theta = 2m\pi \tag{3}$$

where m is an integer. From (3), it can be obtained that the m resonant wavelength is

$$\lambda_m = \frac{BL}{m}. \tag{4}$$

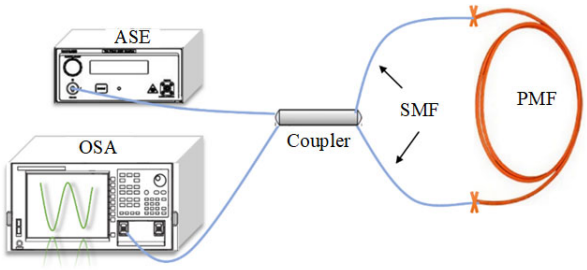

Fig. 1 Schematic diagram of the fiber SI structure (ASE: amplified spontaneous emission light source, SMF: single mode fiber, and OSA: optical spectrum analyzer).

In interferometric fiber sensors, the free spectral range (FSR) of the output spectrum is a key research parameter, and the equation is as follows:

$$\mathrm{FSR} = \frac{\lambda^2}{BL}. \tag{5}$$

It can be seen from (5) that the FSR is inversely proportional to the birefringence coefficient B and the length L of the PMF, and is directly proportional to the working wavelength λ. With the change in external factors (such as the strain, temperature, and stress), the PMF birefringence coefficient B and length L will be adjusted accordingly, which will cause the change of phase difference θ, resulting in the shift of the interference resonance wavelength. The change in phase difference can be described as

$$\Delta\theta = \frac{2\pi}{\lambda}\left[\Delta BL + B\Delta L\right] \tag{6}$$

where $\Delta B = \Delta n_{\mathrm{slow}} - \Delta n_{\mathrm{fast}}$ represents the variation of the PMF birefringence coefficient caused by external factors, Δn_{slow} is the variation of the RI in the slow axis of the PMF, Δn_{fast} is the variation of the RI in the fast axis of the PMF, and ΔL is the change of the PMF length. The shift in the resonant wavelength of the transmission spectrum caused by the change in the phase difference can be described as

$$\Delta\lambda = \frac{\mathrm{FSR}\Delta\theta}{2\pi}. \tag{7}$$

According to (7), changes in external conditions can be detected by recording the movement of the resonant wavelength. In this paper, the PMF is used as the sensing element. When the strain (ε=$\Delta L/L$) is applied, the PMF birefringence coefficient B and length L change, causing the resonant wavelength of the interference spectrum to shift, and the wavelength shift of the SI can be described as

$$\Delta\lambda(\varepsilon) = \lambda(1 + P_e')\varepsilon. \tag{8}$$

Among them, $P_e' = (P_e^f n_{\mathrm{fast}} - P_e^s n_{\mathrm{slow}})/B$ is a constant which describes the variation of birefringence caused by changing strain. P_e^f and P_e^s are constants related the variation of birefringence in the fast axis and slow axis of the PMF, respectively. As can be seen from (8), $\Delta\lambda$ is directly proportional to ε. In addition, PMF shows the high sensitivity to temperature due to the thermo-optical effect and thermal expansion effect of fiber materials. When the temperature changes, the SI wavelength shifts, which can be described as

$$\Delta\lambda(T) = \frac{\lambda}{B(\lambda,T)}\left[\Delta B(\lambda,T)L + B(\lambda,T)\Delta L\right] \tag{9}$$

where $\Delta B(\lambda,T)L$ and $B(\lambda,T)\Delta L$ represent the thermal optical effect and thermal expansion effect, respectively. Because the wavelength shift caused by the thermal expansion effect is two orders of the magnitude smaller than that of the thermal optical effect, the effect of the thermal expansion effect can be ignored. In this paper, the PMF is used as a sensing unit, which is highly sensitive to external factors (the temperature and strain). Due to the difference in RI between the fast axis and slow axis in the PMF, the light will have a specific phase difference in its transmission path, which further causes the interference resonance wavelength in the output spectral signal to shift. Therefore, by monitoring the shift of the resonant wavelength in the SI, the change of external physical parameters can be detected.

2.2.2 Principle of harmonic Vernier effect

The Vernier effect, renowned for its application in calipers, enhances measurement accuracy by

overlapping two scales with slightly different periods [26, 27]. When taking measurement with a caliper, one Vernier scale glides in relation to the other stationary scale. Similarly, the optical Vernier effect employs two interferometers with slightly shifted interferometric frequencies. Ideally, one interferometer serves as a sensor, while the other acts as a stable reference. The basic optical Vernier effect requires two interferometers with slightly offset interference frequencies. In an SI, the interference frequency is adjusted by varying the length of the PMF relative to the interferometer's optical path length. Considering the characteristics of the initial SI, the second interferometer can be tuned to maximize the enhancement provided by the Vernier effect.

The harmonic Vernier effect is the extension of the traditional basic Vernier effect. The harmonic Vernier effect also uses the Vernier method to enhance the sensitivity of the interference sensor. The difference is that the FSR of one interferometer in the harmonic Vernier effect is about an integer multiple of another interferometer FSR. This method effectively reduces the complexity of the Vernier effect sensor preparation. At the same time, with an increase in the harmonic order, the sensitivity amplification factor also doubles, making it possible to break through the limitations of the basic Vernier effect. Based on the harmonic Vernier effect in the fiber sensing structure model (comprising two cascaded SIs, named the reference SI and sensing SI), the PMF lengths in two SIs are related. From FSR (5) for a single SI, the FSR of the basic Vernier effect envelope spectrum can be described as

$$\mathrm{FSR}_{\mathrm{envelope}} = \frac{\mathrm{FSR}_r \times \mathrm{FSR}_s}{\left|\mathrm{FSR}_r - \mathrm{FSR}_s\right|} = \frac{\lambda^2}{B\left|L_r - L_s\right|} \quad (10)$$

where $\mathrm{FSR}_{\mathrm{envelope}}$ is the FSR of the upper envelope of the interference spectrum, FSR_r is the FSR of the upper envelope of the interference spectrum of the reference SI, FSR_s is the FSR of the upper envelope of the interference spectrum of the sensing SI, L_r is the length of the reference SI, and L_s is the length of the sensing SI.

When the FSRs of two SIs are close together, a basic Vernier effect occurs. Suppose that an interferometer optical path is i times of another interferometer optical path, namely $iL_s + L_r$ (i is the harmonic order), which will produce the optical harmonic Vernier effect [22]. In the harmonic Vernier effect, the FSR of the upper envelope can be described as

$$\mathrm{FSR}^i_{\mathrm{envelope}} = \frac{\mathrm{FSR}_r \times \mathrm{FSR}^i_s}{\left|\mathrm{FSR}_r - (i+1)\mathrm{FSR}^i_s\right|} = \frac{\lambda^2}{B\left|L_r - L_s\right|} \quad (11)$$

where $\mathrm{FSR}^i_{\mathrm{envelope}}$ is the FSR of the upper envelope of the interference spectrum for the ith order harmonic Vernier effect, and FSR^i_s is the FSR of the upper envelope of the transmission spectrum of the ith order sensing SI.

According to (11), in the harmonic Vernier effect, the FSR of the upper envelope is independent of the harmonic order. Meanwhile, the FSR expression for the inner envelope can be described as

$$\mathrm{FSR}^i_{\mathrm{harmonic}} = \frac{(i+1)\mathrm{FSR}_r \times \mathrm{FSR}^i_s}{\left|\mathrm{FSR}_r - (i+1)\mathrm{FSR}^i_s\right|} = (i+1)\mathrm{FSR}^i_{\mathrm{envelope}} \quad (12)$$

where $\mathrm{FSR}^i_{\mathrm{harmonic}}$ is the FSR of the inner envelope of the interference spectrum for the ith order harmonic Vernier effect.

As can be seen from (12), the FSR of the inner envelope is i+1 times that of the upper envelope. The magnification factor M of the basic Vernier effect is obtained by calculating the FSR ratio of the outer envelope to a single SI FSR. Therefore, the amplification factor M^i based on the harmonic Vernier effect (using the inner envelope) can be described as

$$M^i = \frac{\mathrm{FSR}^i_{\mathrm{harmonic}}}{\mathrm{FSR}_s} = \frac{(i+1)\mathrm{FSR}_r}{\left|\mathrm{FSR}_r - (i+1)\mathrm{FSR}^i_s\right|} = (i+1)M. \quad (13)$$

As can be seen from (13), the magnification of the harmonic Vernier effect is i+1 times that of the basic Vernier effect.

2.2 Spectral simulation of harmonic Vernier effect

In this paper, the interference spectra based on the basic Vernier effect cascade SI and harmonic

Vernier effect cascade SI are numerically simulated. For the basic Vernier effect, the PMF lengths in the reference interferometer and sensing interferometer are set to 48 cm (marked as PMF1) and 55 cm (marked as PMF2), respectively. In order to generate the harmonic Vernier, the PMF in the sensing interferometer (PMF2) length L_s is set to 55 cm, and the PMF in the reference interferometer (PMF1) length L_r is set to $L_r = 47 + iL_s$ (i=1, 2, and 3). In fact, the condition for the harmonic Vernier effect is that the PMF1 length should be an integer multiple of the PMF2 length plus a certain difference. The smaller the difference is, the more significant the harmonic Vernier effect is. By setting the length of PMF1 to 47 cm, the difference between the PMF1 length and the PMF2 length is reduced, so that the harmonic Vernier effect is more favorable for observation. According to the previous theoretical analysis, to perform the simulation using the Matlab software platform, the resulting basic Vernier effect and harmonic Vernier effect cascade SI output spectrum results of numerical simulation analysis are shown in Fig. 2, and the wavelength range is 1 250 nm–1 650 nm. In the simulation process, the fiber coupler is idealized and the PMF birefringence coefficient B=4.5×10^{-4} is adopted. Figure 2(a) shows the basic Vernier effect, whose upper envelope FSR is 83.96 nm. Figures 2(b)–2(d) show the harmonic Vernier effect; the blue envelope is the upper envelope of the harmonic Vernier effect; the red envelope is the inner envelope of the harmonic Vernier effect. The inner envelope of the Vernier effect for the order i harmonics is obtained by data fitting. Firstly, the maximum values in the harmonic spectrum are divided into i+1 groups, then the maximum values of each group are searched for the peak, and the extreme values are selected for envelope fitting. In addition, it is important to note that the contrast of the inner envelope is higher than that of the outer envelope. This is because the free spectral range of the outer envelope is basically unchanged or has a small range change, while the FSR of the inner envelope increases with an increase in the harmonic order i. In the same wavelength range, the contrast of the outer envelope gradually decreases. Because the higher contrast helps in improving the sensor anti-noise performance, the sensor shows higher stability during the measurement process.

As shown in Fig. 2(b), in the first-order harmonic Vernier effect, the FSR of the upper envelope is 64.5 nm, while the FSR of the inner envelope is 129.5 nm, which is about twice the FSR of the upper envelope. Figure 2(c) illustrates that the second-order harmonic Vernier effect, where the FSR of the upper envelope is 60.0 nm and the FSR of the inner envelope is 180.6 nm, about three times of the FSR of the upper envelope. As shown in Fig. 2(d), the upper envelope FSR of the third-order harmonic Vernier effect is 54.2 nm, and the inner envelope FSR is 217.4 nm, which is about four times of the upper envelope FSR. Considering the small errors caused by measurement and graph labeling, the simulation results are consistent with those analyzed in (12). As can be seen from the simulation spectra of the third-order harmonic cursor effect in Fig. 2(d), the resolution of the spectrum envelope decreases with an increase in the harmonic order, and the resolution of upper envelope is too low for observation. Due to the limitation of the light source wavelength range, a large inner envelope may not be fully displayed, which is not conducive to tracking the shift of the envelope in the spectrum. Therefore, the following measurement and analysis of sensing characteristics of the harmonic Vernier effect do not use the harmonic Vernier effect of the second-order and above. The inner envelope FSR generated by the harmonic Vernier effect exceeds the envelope FSR generated by the basic Vernier effect. Therefore, when the external environment changes slightly, the harmonic Vernier will produce a larger wavelength shift, that is, the sensitivity of the sensor will be further improved, which is of great significance in the field of sensing.

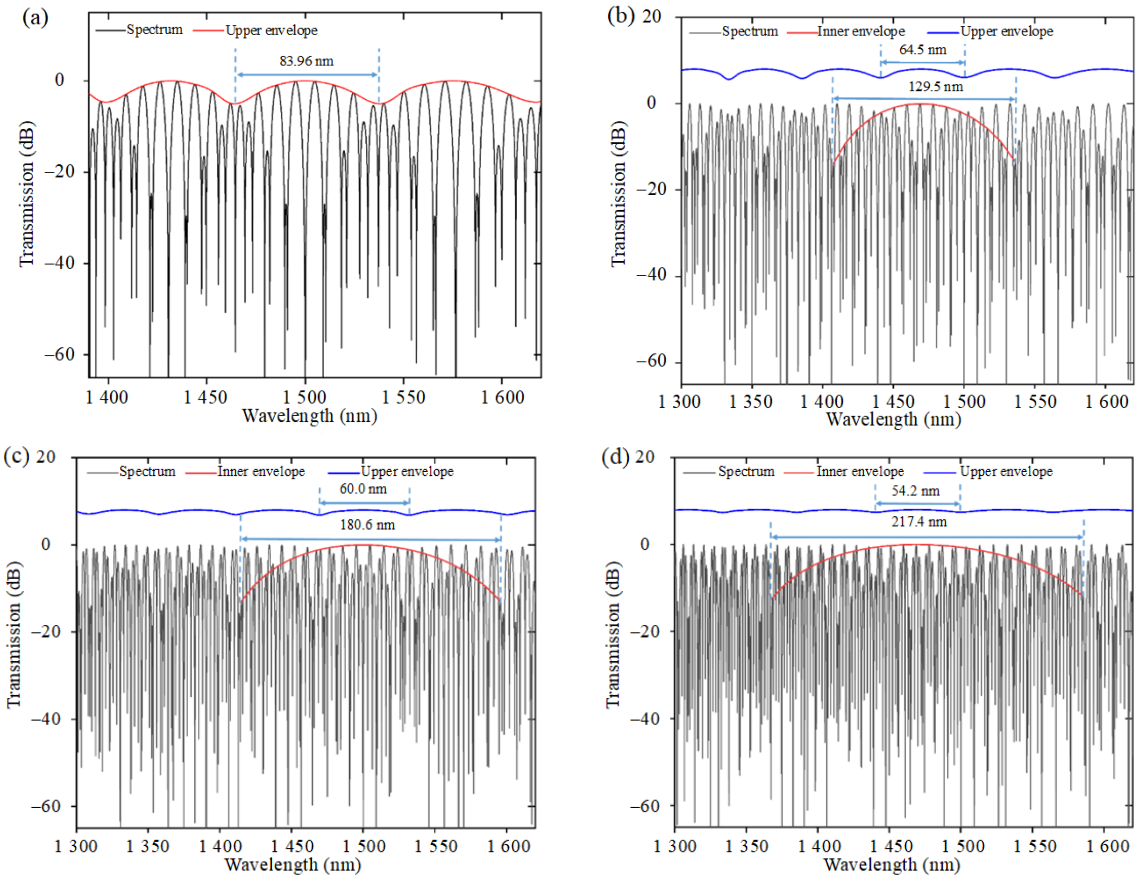

Fig. 2 Spectral simulation in the wavelength range of 1250 nm–1650 nm: (a) basic Vernier effect (PMF1=48 cm and PMF2=55 cm), (b) the first-order harmonic Vernier effect (PMF1=102 cm and PMF2=55 cm), (c) the second-order harmonic Vernier effect (PMF1=157 cm and PMF2=55 cm), and (d) the third-order harmonic Vernier effect (PMF1=212 cm and PMF2=55 cm).

3. Experimental results and discussion

3.1 Structure and construction of sensor system

In the experiment of the harmonic Vernier effect, the PMF (PM#1550/125-18/250-Y, YOFC, China) is selected as the sensing unit, and its cross section is shown in Fig. 3. Three kinds of sensor probes with the lengths of 48 cm, 55 cm, and 102 cm were prepared by the welding mechanism (FSM-100P, Fujikura, Japan). The sensing system with the SI cascade generating harmonic Vernier effect is shown in Fig. 3.

The sensing system mainly consists of two segments of the PMF, two 3 dB couplers, an amplified spontaneous emission light source (ASE, Fiberer, China), and a spectral analyzer (OSA, AQ6370D, YOKOGAWA, Japan) with a wavelength range of 1 250 nm–1 650 nm and a minimum resolution of 0.02 nm. In this system, two SIs are composed of different lengths PMFs, respectively, and the basic Vernier effect and harmonic Vernier effect are generated in a cascade way to improve the sensitivity. The incident light signal emitted by the ASE first passes through the reference interferometer, then enters the sensing interferometer, and the final interference light signal is received by the OSA. In a single Sagnac loop, the length of the PMF is 55 cm. For the basic Vernier sensing device, set PMF1=48 cm and PMF2=55 cm. For the first-order harmonic Vernier effect, set PMF1=102 cm and PMF2=55 cm.

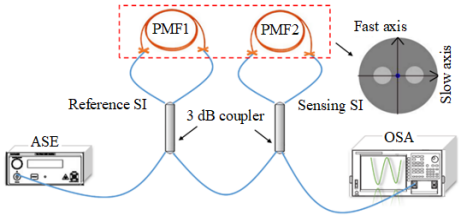

Fig. 3 Schematic diagram of cascaded SI sensing system based on harmonic Vernier effect.

3.2 Sensing characteristics testing and analysis

First, the cascaded SI output spectra based on the basic Vernier effect and the first-order harmonic Vernier effect in the wavelength range of 1250 nm–1650 nm are tested at room temperature. As shown in Fig. 4(a), the FSR of the basic Vernier effect envelope spectrum is 83.52 nm, while the FSR of a single sensing SI is 9.76 nm, so the calculated magnification is about 8.6 times. According to the theory of harmonic generation, the lengths of PMF1 and PMF2 are changed, and the spectrum of the harmonic Vernier effect as shown in Fig. 4(b) is obtained.

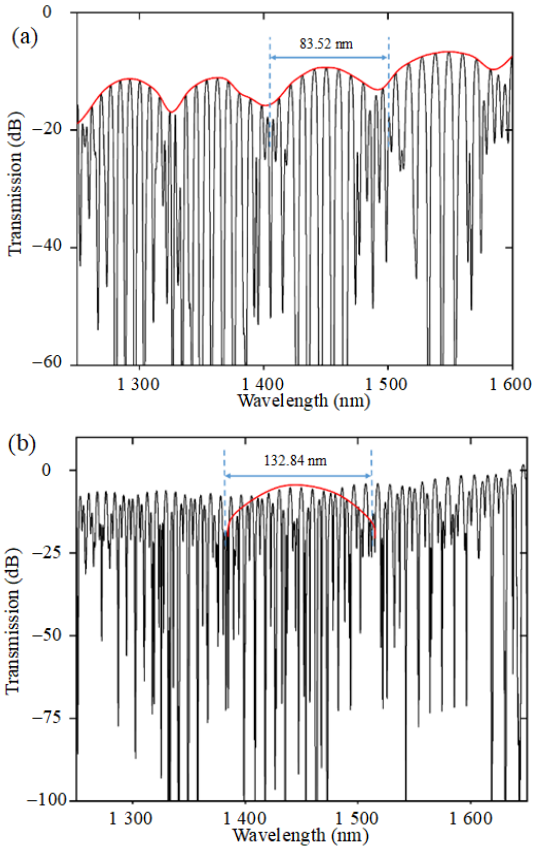

Fig. 4 Experimental spectra: (a) the basic Vernier effect (PMF1=48 cm and PMF2=55 cm) and (b) the first-order harmonic Vernier effect (PMF1=102 cm and PMF2=55 cm).

The inner envelope FSR of the first-order harmonic Vernier effect is 132.84 nm, which shows the magnification of 13.6 times compared with that of a single SI. This magnification is consistent with the magnification of the basic Vernier effect and the harmonic Vernier effect calculated in (13). Next, in order to verify that the harmonic Vernier effect can further improve the sensitivity of the fiber sensor, the cascaded SI strain and temperature sensing performance based on the basic Vernier effect and the first-order harmonic Vernier effect are analyzed experimentally.

3.2.1 Strain sensing characteristic

In order to study the strain sensing characteristics of the basic Vernier effect and first-order harmonic Vernier effect formed by the cascade of two Sagnac loops, the PMF2 is fixed on the displacement platform by using a fiber-optic fixture, and the strain is applied to the PMF2 by moving the displacement platform, while ensuring that the PMF1 is fixed to reduce the influence of other factors on the experimental results. In the experimental setup, the initial distance between the two displacement stations is 20 cm, and the displacement stations are set to move 50 μm each time; that is, the strain step is 250 με. Figures 5(a) and 5(b) show the cascade SI spectral changes of the basic Vernier effect and first-order harmonic Vernier effect during the strain increase from 0 με to 1 250 με. It can be seen that with an increase in the strain, the cascade SI envelope resonance wavelengths of the basic Vernier effect and first-order harmonic Vernier effect are red-shifted, but the strain sensitivity is different.

Figure 6 shows the linear fitting curve of the envelope resonance wavelength increasing with the strain for the cascade SI basic Vernier effect and first-order harmonic Vernier effect. The linear fitting equations based on the cascade SI basic Vernier effect and first-order harmonic Vernier effect are y=61.93x+1 467.08 and y=146.35x+1 353.65, respectively. The linear fitting coefficients are 0.996 67 and 0.997 10, respectively. Thus, the strain sensitivity of these two structures is 61.93 pm/με and 146.35 pm/με. According to [28], the sensitivity of a single SI is 8.13 pm/με in the strain range of 0 με–1 250 με. Compared to a single SI, the sensor

designed with the first-order harmonic Vernier effect achieved a significant 18 times increase in strain sensitivity. In addition, when compared with the sensor constructed with basic Vernier effect, the first-order harmonic Vernier effect based on the cascade SI also shows a 2.3 times increase in strain sensitivity. Considering the minimum resolution of the OSA used in this paper is 0.02 nm, the strain resolution of the fiber sensor based on the basic Vernier effect and first-order harmonic Vernier effect can be calculated as 0.322 94 με and 0.136 65 με, respectively. Limited by the wavelength range of the ASE, the strain detection range based on the cascade SI first-order harmonic Vernier effect is 2.73 mε. In the presentation of experimental results, each data point represents the average of five times of independent measurement, and the error bar represents the standard deviation from that average.

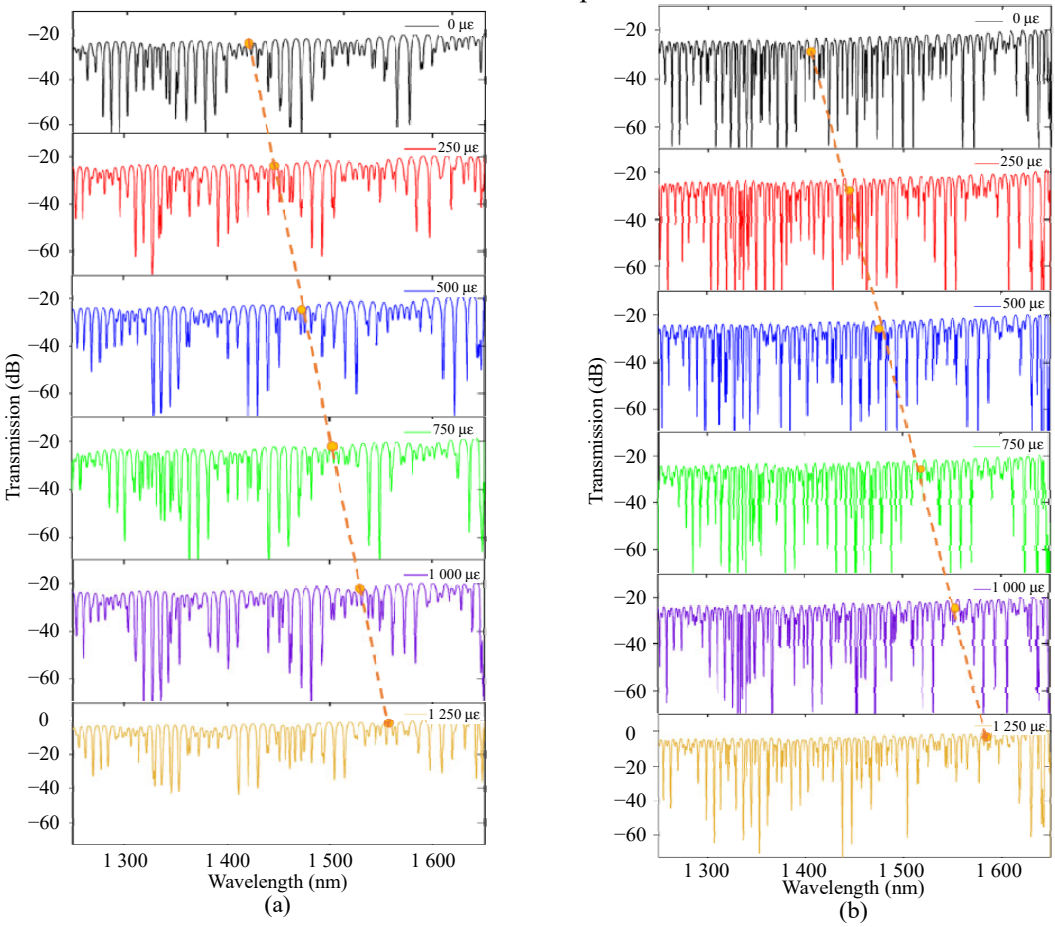

Fig. 5 Transmission spectra under strains: (a) the basic Vernier effect and (b) the first-order harmonic Vernier effect.

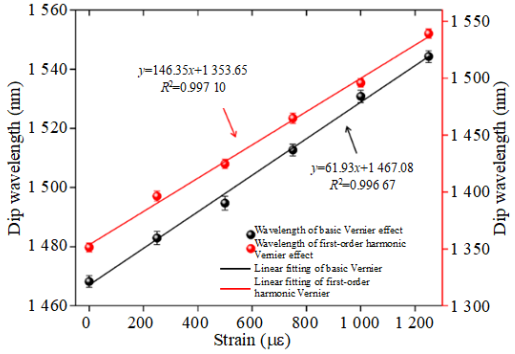

Fig. 6 Strain fitting curves of the basic Vernier effect and first-order harmonic Vernier effect.

3.2.2 Temperature sensing characteristic

In addition, the properties of the basic Vernier effect and first-order harmonic Vernier effect in temperature sensing are also studied. The PMF2 is placed in a temperature control chamber with a resolution of 0.1 ℃, while the PMF1 is fixed on the bench and placed under constant temperature conditions to avoid cross crosstalk. The sensor probe (i.e., PMF2) is heated from 27 ℃ to 32 ℃ at a step

of 1 ℃. The cascaded SI spectra of the basic Vernier effect and first-order harmonic Vernier effect as a function of temperature are shown in Figs. 7(a) and 7(b). The wavelength of envelope spectrum resonance based on the basic Vernier effect and first-order harmonic Vernier effect blue-shifts with an increase in temperature, but the sensitivity of temperature is different. According to [28], the blue-shift range of a single SI least changes with temperature; the harmonic envelope based on the first-order harmonic Vernier effect maximally changes the blue-shift range with temperature; the envelope based on the basic Vernier effect changes the blue shift range moderately.

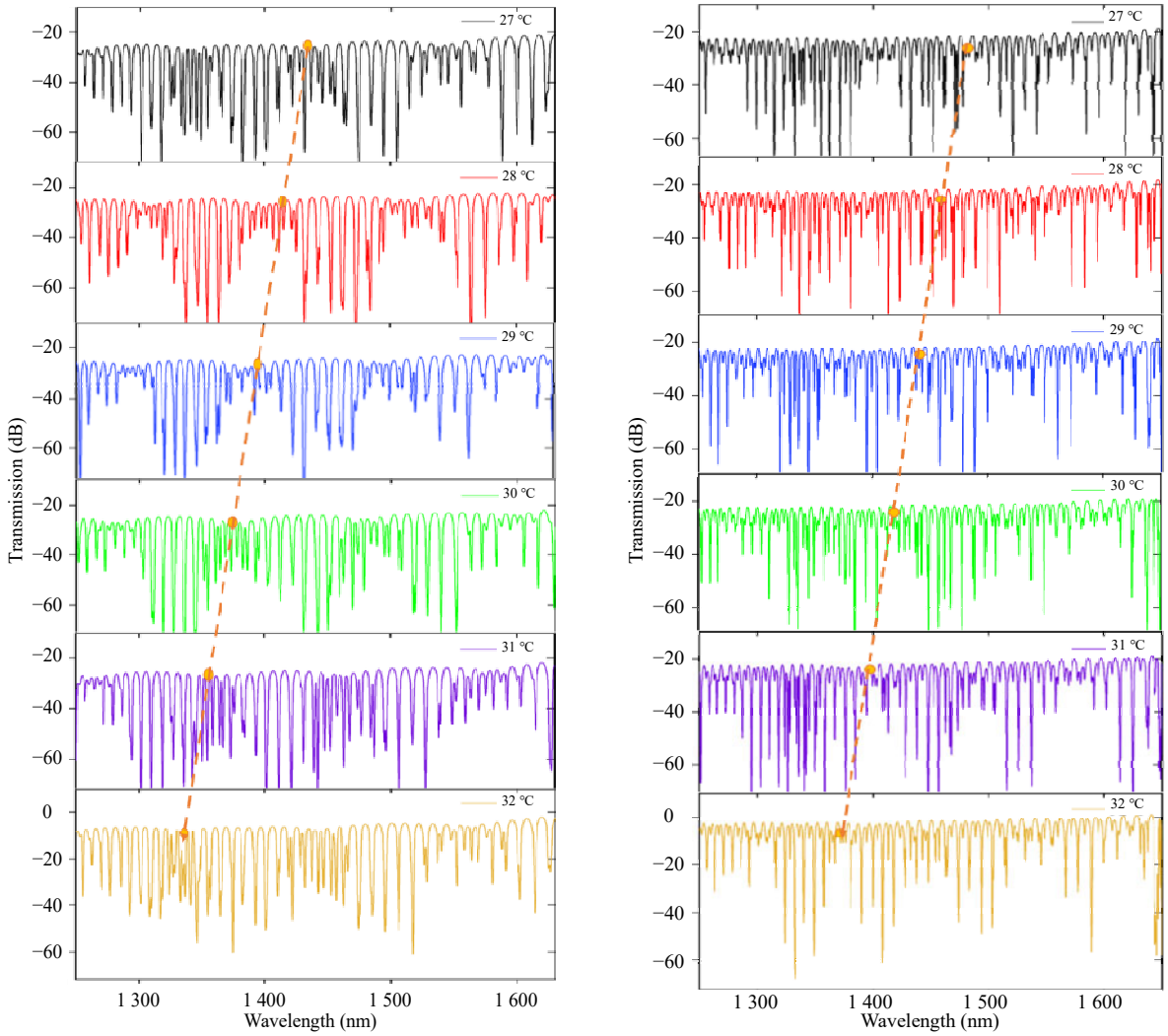

Fig. 7 Transmission spectra under different temperature: (a) the basic Vernier effect and (b) the first-order harmonic Vernier effect.

Figure 8 shows the linear fitting curve of the envelope resonance wavelength changing with temperature for the cascaded SI basic Vernier effect and first-order harmonic Vernier effect. The linear fitting equations based on the cascaded SI basic Vernier effect and first-order harmonic Vernier effect are $y=-14.29x+1\,923.06$ and $y=-24.92x+2\,051.67$, respectively. The linear fitting coefficients are 0.998 60 and 0.997 74, respectively. Therefore, the temperature sensitivity values of these two structures are −14.29 nm/℃ and −24.92 nm/℃, respectively. At the same time, according to [28], the sensitivity of a single SI in the temperature range of 27 ℃–32 ℃ is −1.51 nm/℃. Compared to a single SI fiber sensor, the sensor designed with the first-order harmonic Vernier effect achieves a

significant increase in temperature sensitivity of about 16.5 times. Furthermore, the sensor based on first-order harmonic Vernier effect has a 1.74 times increase in temperature sensitivity compared to the sensor based on basic Vernier effect. Considering the minimum resolution of the OSA used in this paper of 0.02 nm, the temperature resolution of the fiber sensor based on the basic Vernier effect and first-order harmonic Vernier effect can be calculated as 0.001 40 ℃ and 0.000 82 ℃, respectively. Limited by the wavelength range of the ASE, the temperature detection range based on the cascade SI first-order harmonic Vernier effect is 16.05 ℃. In the experimental results, each data point represents the average of five times of independent measurement, and the error bar represents the standard deviation from that average. Although the first-order harmonic Vernier effect based on the cascade SI is only detected in the temperature range of 27 ℃–32 ℃ in this temperature experiment, it has ultra-high temperature sensitivity and temperature resolution, which can be used in monitoring scenarios requiring high temperature accuracy. Because the fiber sensor based on the harmonic Vernier effect has a wide FSR, the temperature range that can be detected is limited. When the wavelength shift is too large, it will exceed the available wavelength range of the ASE or the wavelength measurement range of the OSA.

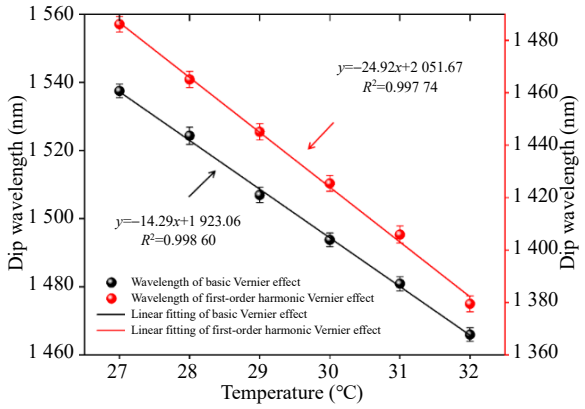

Fig. 8 Temperature fitting curves of the basic Vernier effect and first-order harmonic Vernier effect.

3.3 Strain/temperature stability analysis

Stability is the key index to evaluate the sensor performance, so the stability is analyzed experimentally in this paper. For the stability test of the strain, the probe PMF2 is placed on the displacement table at room temperature, and then the strain of 1 000 με is applied, and the resonant wavelength is recorded every 10 minutes under this condition for 80 minutes. During the test period, the PMF1 is fixed on the test table to reduce the influence of other factors on the test results. Similarly, for temperature stability, the probe PMF2 is placed in the temperature control chamber, keeping at 30 ℃ for 80 minutes, and the resonant wavelength is recorded every 10 minutes. During the temperature stability test, the PMF1 is placed at room temperature to prevent temperature crosstalk from affecting the experimental results. The results of the strain and temperature stability are shown in Fig. 9. The maximum error between the resonant wavelength and the average value (1 449.44 nm) at the 1 000 με strain condition is 0.04 nm. Therefore, the measurement error at the 1 000 με strain condition is about 0.27 με (0.04/0.146 35=0.27 με). Small errors may be caused by small external disturbances during the experiment. At 30 ℃, the maximum wavelength deviation between the resonant wavelength and the average value (1 512.46 nm) is 0.06 nm. Therefore, the error at 30 ℃ is 0.003 ℃ (0.06/24.92=0.002 ℃). The small error may be caused by the small temperature disturbance in the temperature control chamber during the experiment. Based on the stability test results, the sensor shows high stability in strain and temperature measurement.

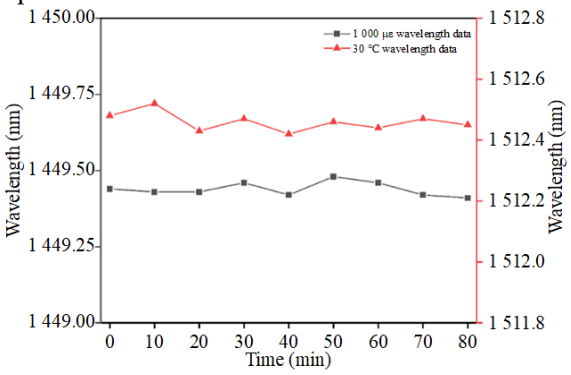

Fig. 9 Strain and temperature stability results of the first-order harmonic Vernier effect.

In Table 1, the proposed sensor based on the harmonic Vernier effect is compared with existing fiber sensors in terms of strain and temperature measurement performance. The sensitivity of fiber-optic temperature sensors based on various structures of the harmonic Vernier effect proposed in [29–32] is low and cannot meet the needs of high sensitivity applications. The strain sensor based on the harmonic Vernier effect proposed in [33] has the strain sensitivity of 20.38 pm/με, which means that the sensitivity can be improved. The parallel FPI fiber sensor based on the harmonic Vernier effect proposed in [34] can realize the dual-parameter detection of the strain and temperature, and the strain and temperature sensitivity is 178.75 pm/με and 0.012 8 nm/℃, respectively, but their sensitivity is low and cannot meet the requirements of the high sensitivity measurement field. The cascade FPI fiber temperature sensor based on the harmonic Vernier effect proposed in [35] shows a wide working range, with the sensitivity of 0.109 72 nm/℃, which will limit its further practical application. In contrast, the two cascade SIs proposed in this paper can realize the sensor measurement of the strain and temperature based on the first-order harmonic Vernier effect, showing higher sensitivity than other fiber-optic sensors listed in Table 1. Because of its simple structure and low cost, the sensor presented in this paper shows the wide application potential in engineering and medical fields of high precision measurement.

Table 1 Performance comparison between this sensor and existing fiber optic sensors.

Ref.	Sensor type	Sensing parameter	Range (℃ or με)	Sensitivity (nm/℃ or pm/με)
[29]	Cascade PMF-SIs	Temperature	30–70	3.66
[30]	Cascade PMF-SIs	Temperature	30–37	53.3
[31]	PDMS+FPI	Temperature	40–60	3.4
[32]	Cascade FPI and MI	Temperature	41–44	19.22
[33]	Cascade MMI-MZI	Strain	0–1 356.5	20.38
[34]	Parallel FPIs	Strain	0–200	178.75
		Temperature	20–900	0.012 8
[35]	Cascade FPIs	Temperature	25–800	0.109 72
This paper	Cascade SIs	Strain	0–1 250	146.35
		Temperature	27–32	24.92

4. Conclusions

In this paper, a strain and temperature sensor based on the cascade SI harmonic Vernier effect is proposed. Through simulation and experimental research, it is found that the basic Vernier effect can be realized when the PMF lengths of two SIs are slightly different, and the first-order harmonic Vernier effect can be further realized when the lengths of two PMFs are approximately multiple. The sensor device composed of the harmonic Vernier effect has a larger FSR of the output spectrum and higher measurement sensitivity. Compared with a single SI, the strain sensitivity based on the basic Vernier effect is improved from 8.13 pm/με to 61.93 pm/με, with the magnification of 7.6 times, and the temperature sensitivity is improved from 1.51 nm/℃ to 14.29 nm/℃, with the magnification of 9.4 times. The strain sensitivity of the sensor based on the first-order harmonic Vernier effect is increased from 8.13 pm/με to 146.35 pm/με. The temperature sensitivity is increased from 1.51 nm/℃ to 24.92 nm/℃, and the magnification is 16.5 times. Therefore, sensors based on the harmonic Vernier effect can significantly improve the sensitivity of strain and temperature measurement. In addition, the research on stability based on the harmonic Vernier effect shows that the sensor has good strain and temperature stability, which has the wide application potential in strain and temperature measurement.

Acknowledgment

This work was supported by the National Key Research and Development Program of China (Grant No. 2023YFB3209500), Shenzhen Science and Technology Program, China (Grant No. JCYJ20220818095800001), China Postdoctoral Science Foundation (Grant No. 2024T170579), National Natural Science Foundation of China (Grant No. 62374111), and Guangdong Basic and Applied Basic Research Foundation, China (Grant No. 2024A1515010164).

Declarations

Conflict of Interest Yiping WANG is an editorial board member for Photonic Sensors and was not involved in the editorial review, or the decision to publish this article. All authors declare that there are no competing interests.

Permissions All the included figures, tables, or text passages that have already been published elsewhere have obtained the permission from the copyright owner(s) for both the print and online format.

References

[1] E. F. Seraji and F. Asghari, "Tunable optical filter based on Sagnac phase-shift using single optical ring resonator," *Optics & Laser Technology*, 2009, 42(1): 115–119.

[2] H. Arianfard, J. Y. Wu, S. Juodkazis, and D. J. Moss, "Advanced multi-functional integrated photonic filters based on coupled Sagnac loop reflectors," *Journal of Lightwave Technology*, 2021, 39(5): 1400–1408.

[3] N. Kumar and K. Ramachandran, "Dynamic spectral maneuvering by fiber Sagnac loop filter," *Optics & Laser Technology*, 2014, 63: 144–147.

[4] S. L. Pu, L. F. Luo, J. L. Tang, L. M. Miao, and X. L. Zeng, "Ultrasensitive refractive-index sensors based on tapered fiber coupler with Sagnac loop," *IEEE Photonics Technology Letters*, 2016, 28(10): 1073–1076.

[5] Z. X. Shi, J. B. Zhang, L. Yang, H. Wu, Y. Ni, J. Gong, *et al*., "Miniature optical correlator in a single-nanowire Sagnac loop," *ACS Photonics*, 2020, 7(11): 3264–3269.

[6] B. Stéphane, B. Michael, P. Krishnan, D. Michel, and S. K. Gordon, "Pickup suppression in Sagnac-based fiber-optic acoustic sensor array," *Journal of Lightwave Technology*, 2006, 24(7): 2889–2897.

[7] S. Moseley, N. Scaramuzza, J. Tasson, and M. L. Trostel, "Lorentz violation and Sagnac gyroscopes," *Physical Review D*, 2019, 100(6): 064031.

[8] M. Mohammadi, M. Seifouri, and S. Olyaee, "The rotation sensing based on the Sagnac effect in silicon-integrated optical gyroscope with noise considerations," *Optical and Quantum Electronics*, 2024, 56: 995.

[9] M. Capezzuto, G. Gaudiosi, L. Nardone, E. D'Alema, D. D'Ambrosio, R. Manzo, *et al*., "Fiber-optic gyroscope for rotational seismic ground motion monitoring of the Campi Flegrei volcanic area," *Applied Optics*, 2024, 63(16): 4226–4233.

[10] H. X. Jia, J. M. Wheeler, T. Iantosca, and M. Digonnet, "Low-drift fiber-optic gyroscope interrogated with multiple broadened semiconductor lasers," *Journal of Lightwave Technology*, 2024, 42(13): 4666–4673.

[11] X. Y. Dong, H. Y. Tam, and P. Shum, "Temperature-insensitive strain sensor with polarization-maintaining photonic crystal fiber based Sagnac interferometer," *Applied Physics Letters*, 2007, 90(15): 151113.

[12] G. Kim, T. Cho T, K. Hwang, K. Lee, K. S. Lee, Y. G. Han, *et al*., "Strain and temperature sensitivities of an elliptical hollow-core photonic bandgap fiber based on Sagnac interferometer," *Optics Express*, 2009, 17(4): 2481–2486.

[13] Y. F. Zhao, M. L. Dai, Z. M. Chen, X. Y. Liu, M. S. Gandhi, Q. Li, *et al*., "Ultrasensitive temperature sensor with Vernier-effect improved fiber Michelson interferometer," *Optics Express*, 2021, 29(2): 1090–1101.

[14] H. L. Chen, X. P. Zhu, C. Jiang, H. Li, X. S. Guo, and S. M. Sun, "High sensitivity temperature and pressure sensor based on cascaded Fabry-Perot and Sagnac interferometers," *Instrumentation Science & Technology*, 2022, 50(4): 422–436.

[15] Z. C. Ding, Z. W. Tan, P. K. Zhan, and L. W. Zhang, "Highly sensitive temperature sensor based on cascaded HiBi-FLMs with the Vernier effect," *Journal of the Optical Society of America B*, 2020, 37(7): 1948–1955.

[16] X. L. Jia, X. F. Zhou, M. H. Bi, G. W. Yang, M. M. Hu, and T. S. Wang, "High-sensitivity optical fiber temperature sensor of cascaded FSI and MZI based on Vernier effect," *Optical Fiber Technology*, 2021, 65: 102625.

[17] H. F. Lin, F. F. Liu, H. Y. Guo, A. Zhou, and Y. T, Dai, "Ultra-highly sensitive gas pressure sensor based on dual side-hole fiber interferometers with Vernier effect," *Optics Express*, 2018, 26(22): 28763–28772.

[18] T. Nan, B. Liu, Y. F. Wu, J. F. Wang, Y. Y. Mao, L. L. Zhao, *et al*., "Ultrasensitive strain sensor based on Vernier-effect improved parallel structured fiber-optic Fabry-Perot interferometer," *Optics Express*, 2019, 27(12): 17239–17250.

[19] S. X. Zhang, Y. Liu, Y. J. Zhao, A. Zhou, and L. B. Yuan, "Bending sensor with parallel fiber Michelson interferometers based on Vernier-like effect," *Optics & Laser Technology*, 2019, 120: 105679.

[20] A. D. Gomes, M. S. Ferreira, J. Bierlich, J. Kobelk,

M. Rothhardt, H. Bartelt, *et al*., "Optical harmonic Vernier effect: a new tool for high performance interferometric fiber sensors," *Sensors*, 2019, 19(24): 5431.

[21] A. D. Gomes, M. S. Ferreira, J. Bierlich, J. Kobelk, M. Rothhardt, H. Bartelt, *et al*., "Hollow microsphere combined with optical harmonic Vernier effect for strain and temperature discrimination," *Optics & Laser Technology*, 2020, 127: 106198.

[22] X. M. Yang, S. Wu, H. H. Cheng, J. W. Ma, S. Wang, S. H. Liu, *et al*., "Simplified highly-sensitive gas pressure sensor based on harmonic Vernier effect," *Optics & Laser Technology*, 2021, 140: 107007.

[23] C. H. Luo, X. X. Chen, and S. Wu, "Ultrasensitive fiber-based gas pressure sensor based on harmonic Vernier effect with enhanced contrast," *Optics & Laser Technology*, 2022, 156: 108532.

[24] M. F. He, B. B. Zhu, and Z. X. Zhang, "High sensitivity temperature sensor based on harmonic Vernier effect," *Photonic Sensors*, 2023, 13(2): 230204.

[25] L. Y. Shao, Y. Luo, Z. Y. Zhang, X. H. Zou, B. Luo, W. Pan, *et al*., "Sensitivity-enhanced temperature sensor with cascaded fiber optic Sagnac interferometers based on Vernier-effect," *Optics Communications*, 2015, 336: 73–76.

[26] W. J. Zhang, X. Q. Wu, C. Zuo, L. Gui, J. H. Shi, X. N. Zhao, *et al*., "Highly sensitive temperature and strain sensor based on fiber Sagnac interferometer with Vernier effect," *Optics Communications*, 2022, 506: 127543.

[27] A. D. Gomes, H. Bartelt, and O. Frazão, "Optical Vernier effect: recent advances and developments," *Laser & Photonics Reviews*, 2021, 15(7): 2000588.

[28] K. G. Liu, X. Ding, Y. Li, X. J. Liu, and Q. Xiao, "Dual-parameter sensing of parallel fiber Sagnac interferometer based on vernier effect," *IEEE Sensors Journal*, 2023, 23(7): 6769–6778.

[29] S. Liu, G. W. Lu, D. Y. Lv, M. M. Chen, and Z. X. Zhang, "Sensitivity enhanced temperature sensor with cascaded Sagnac loops based on harmonic Vernier effect," *Optical Fiber Technology*, 2021, 66: 102654.

[30] L. Q. Xie, M. M. Chen, and Z. X. Zhang, "Simplified highly sensitive temperature sensor based on harmonic Vernier effect," *Applied Physics B*, 2022, 128(8): 158

[31] L. Chen, J. J. Tian, Q. Wu, and Y. Yao, "Ultrahigh sensitivity temperature sensor based on harmonic Vernier effect," *IEEE Sensors Journal*, 2022, 23(1): 381–388.

[32] W. L. Yang, R. Pan, L. Y. Zhang, Y. Q. Yang, L. J. Li, S. Yu, *et al*., "Highly sensitive fiber-optic temperature sensor with compact hybrid interferometers enhanced by the harmonic Vernier effect," *Optics Express*, 2023, 31(9): 14570–14582.

[33] P. Yang, S. C. Jiang, Z. H. Wang, X. R. Peng, and B. J. Peng, "Enhancing sensor strain sensitivity via simulated reference arm for optical harmonic Vernier effect," *IEEE Sensors Journal*, 2023, 23(22): 27375–27381.

[34] Z. R. Li, W. J. Dang, J. X. Dan, K. Z. Jin, P. Y. Nan, G. G. Xin, *et al*., "High-sensitivity interferometric high-temperature strain sensor based on optical harmonic Vernier effect," *Optical Fiber Technology*, 2023, 79: 103361.

[35] S. Y. Lin, F. Wang, Y. C. Qu, X. P. Han, and Y. D. Zhang, "High-temperature measurement based on highly-sensitive miniature cascaded FPIs and the harmonic Vernier effect," *Measurement*, 2023, 221: 113456.